An Atomic Level Model for the Interactions of Molybdenum Nitrogenase with Carbon Monoxide, Acetylene, and Ethylene†

Marcus C. Durrant*

Computational Biology Group, John Innes Centre, Norwich Research Park, Colney Lane, Norwich NR4 7UH, UK

Received December 22, 2003; Revised Manuscript Received March 15, 2004

ABSTRACT: A combination of density functional theory and molecular mechanics calculations has been used to study the possible interactions of CO, C_2H_2, and C_2H_4 with the central Fe and terminal Mo sites of the iron−molybdenum cofactor of nitrogenase. The most favorable binding mode for CO on the central section of the FeMoco appears to be end-on to a single Fe and results in a change from high to low spin for the ligating Fe atom. If a coordination site for CO is available on the Mo, this becomes the preferred CO binding site. Calculated ν(CO) infrared frequencies are compared with the experimental values given in the literature. C_2H_2 binds weakly in a side-on orientation to a single Fe site; addition of a single H^+/e^- couple to the substrate results in spontaneous migration of the resulting -CH═CH_2 group from Fe to a central S atom of the cofactor. Further reduction liberates C_2H_4 or alternatively can give an S═$CHCH_3$ intermediate, which then goes on to produce C_2H_6. A model for C_2H_2 reduction by nitrogenase is proposed, based on the results of the calculations and the extensive literature on this process.

Biological nitrogen fixation is mediated by a class of enzymes known as nitrogenases. Several distinct nitrogenases are known and all contain iron/sulfur-based cofactors (*1*), but the most extensively characterized to date is molybdenum nitrogenase, so-called because it contains the additional transition metal Mo. This enzyme consists of two component proteins; the Fe protein (component 2) is a homodimer of ∼64 kDa, contains an Fe_4S_4 cubane, and acts as a specific electron donor to the ∼230 kDa MoFe protein (component 1). The MoFe protein is an $\alpha_2\beta_2$ tetramer and contains two unique metal−sulfur clusters. The P-clusters, stoichiometry Fe_8S_7, appear to act as internal electron relays to the iron−molybdenum cofactor (FeMoco,[1] stoichiometry $MoFe_7S_9N$·homocitrate), which is thought to contain the active site (*2*). When dithionite is used as the primary reductant in vitro, electron transfer to component 1 is accomplished by the association and dissociation of component 2, and is accompanied by the hydrolysis of ATP. The X-ray crystal structures of both component proteins have been described (*3*−*5*). The very latest X-ray crystal structure, obtained at 1.16 Å resolution (*6*), has revealed an important omission from all the earlier work in that the FeMoco contains an additional light atom within its central Fe_6 prism (Figure 1). Although the nature of the central atom could not be precisely defined, the most likely candidate from the crystallography appears to be N, and this is supported by recent theoretical studies (*7*−*10*). Prior to the detection of the central light atom, the oxidation state composition of FeMoco at the dithionite-reduced, resting state level was thought to be either $[Fe^{3+}Fe^{2+}{}_6Mo^{4+}]$ (*11*, *12*) or $[Fe^{3+}{}_3Fe^{2+}{}_4Mo^{4+}]$ (*13*). Following the revision of the X-ray crystal structure, the consensus view from experimental and theoretical studies is that the second assignment is the correct one (*7*−*10*, *14*).

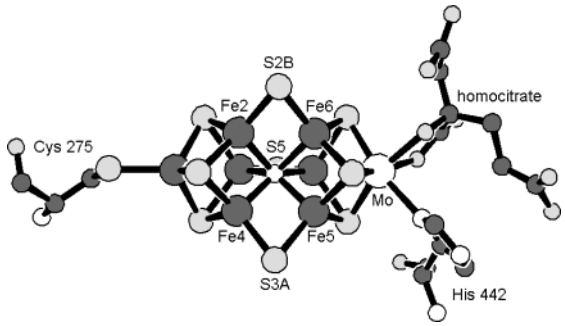

FIGURE 1: X-ray crystal structure of FeMoco from Av1, showing the amino acid ligands and the labeling of the central S and Fe atoms. The unlabeled Fe atoms are Fe3 (left) and Fe7 (right).

In addition to its biological function of N_2 reduction, nitrogenase interacts with a considerable variety of small molecules, including acetylene, ethylene, and carbon monoxide. At ambient temperature, wild-type Mo nitrogenase reduces acetylene exclusively to ethylene, although a small amount of ethane is also obtained at 50 °C (*15*), and some mutant forms of the enzyme also give ethane as a secondary product (*16*−*20*). Reduction of C_2H_2 in D_2O gives *cis*-$C_2H_2D_2$ as the primary product, although again mutant forms of the enzyme can be less selective, giving enhanced levels of *trans*-$C_2H_2D_2$ (*18*, *20*). Ethylene is also a substrate for Mo nitrogenase (*2*), although much inferior to acetylene; on using a 5-fold excess of Kp1 over Kp2, C_2H_4 reduction accounted for no more than 1% of the total electron flux (*21*). Carbon monoxide is not itself a substrate for nitroge-

† Support provided by the Biotechnology and Biological Sciences Research Council, UK.

* Telephone: +44 (0)1603 450704. Fax: +44 (0)1603 450021. E-mail: marcus.durrant@bbsrc.ac.uk.

[1] Abbreviations: Av1, Kp1, MoFe proteins from *A. vinelandii* and *K. pneumoniae*, respectively; Kp2, iron protein from *K. pneumoniae*; DFT, density functional theory; ENDOR, electron nuclear double resonance; EPR, electron paramagnetic resonance; FeMoco, iron−molybdenum cofactor; imH, imidazole; MM, molecular mechanics; NS3, $N(CH_2CH_2S)_3^{3-}$ ligand; SF-FTIR, stopped-flow Fourier transform infrared.

10.1021/bi036300l CCC: $27.50
Published on Web 04/30/2004

nase, but is an inhibitor of the reduction of all known substrates except H^+. A number of experiments have revealed a complicated relationship between the interactions of C_2H_2, C_2H_4, and CO with the FeMoco. Thus, kinetic studies on *Klebsiella pneumoniae* nitrogenase indicated that C_2H_2 and CO can bind simultaneously to nitrogenase (*22*). Christiansen et al. concluded from work on an Av1 α-Ser^{69} mutant that the FeMoco has both high and low affinity binding sites for C_2H_2 ($K_m \sim 0.007$ and ~ 0.14 Atm, respectively), both of which can also bind CO (*23*, *24*). Kinetic studies on an Av1 α-His^{277} mutant led Shen et al. to a model involving simultaneous binding of one molecule of CO and two of C_2H_2 at the FeMoco (*25*). EPR studies on an Av1 α-Gln^{195} mutant gave spectra indicative of two C_2H_2 ligands bound to the FeMoco (*26*, *27*), while studies on mutant Av1 proteins (α-Asn^{195}, α-Gln^{195}, α-Lys^{191}) led Fisher et al. to conclude that nitrogenase can simultaneously bind either two molecules of C_2H_4 or one of C_2H_4 and one of CO (*18*). Finally, EPR/ENDOR studies have shown that wild-type nitrogenase can simultaneously bind two CO ligands at the FeMoco during turnover (*28*, *29*), while SF-FTIR of nitrogenase under turnover conditions shows a single band at 1904 cm^{-1} under low CO concentrations and a more complicated set of bands at higher CO concentrations (*30*). Recently, Dean and coworkers have described the alkyne-reducing properties of Av1 mutants involving changes to the wild-type residues α-Gly^{69} and α-Val^{70} (*24*, *31*, *32*). These studies also indicated that nitrogenase possesses two acetylene reduction sites, with markedly different K_m values. Elimination of the high affinity C_2H_2 site in an α-Ser^{69} mutant significantly impairs the enzyme's ability to reduce C_2H_2 without greatly affecting its N_2-reducing properties. Conversely, replacing α-Val^{70} with Ala or Gly gives an enzyme that can reduce propyne, a very poor substrate for the wild-type enzyme, and even propargyl alcohol, HC≡CCH$_2$OH.

Another line of attack that has been used to probe the reactivity of the FeMoco stems from the development of a method for the extraction of the intact cluster from the protein (*2*). In the presence of an appropriate primary reductant, extracted FeMoco catalyzes the reduction of C_2H_2 to C_2H_4 and C_2H_6, while C_2H_4 remains a very poor substrate (*33*). As with the whole enzyme, reduction of C_2D_2 was found to give predominantly *cis*-$C_2H_2D_2$, and C_2H_2 was found to bind cooperatively to at least two sites on the FeMoco (*34*). Electrochemical studies on extracted FeMoco showed that the cluster binds CO upon reduction below the dithionite-reduced level (*14*, *35*); the results were interpreted in terms of binding of one or two CO ligands to the central Fe sites and a third CO at the Mo, which lacks its normal histidine ligand.

In previous theoretical studies, I used density functional theory (DFT) and molecular mechanics (MM) studies in conjunction with the available experimental data to develop a paradigm for nitrogenase reactivity with respect to H^+, N_2, and H_2 (*36*−*38*). This paper deals with the extension of the model to the alternative substrates C_2H_2 and C_2H_4, and the inhibitor CO.

MATERIALS AND METHODS

MM calculations were done with Chem-X (*39*) and Insight II (*40*) software. All Chem-X calculations were performed on crystal structures lacking the central light atom; its inclusion would not change the results, since it has no steric effect outside the FeMoco core cluster. The standard Chem-X atom parameter set was modified to accommodate the FeMoco by including parameters for Fe and Mo, as follows. Three- and four-coordinate Fe and six-coordinate Mo atoms were defined, and bond lengths and angles were specified based on the crystal structure geometries (*4*, *5*). To model the sideways-bound C_2H_2 ligands, a dummy atom X was defined at the centroid of the ligand and used to attach it to the Fe atom. The optimum parameters were specified as Fe−X = 2.32 Å, S−Fe−X = 80°, Fe−X−C = 90°. For the Fe−CH=CH$_2$ group, optimum parameter values were specified as Fe−C = 2.00 Å, S−Fe−C = 80°, Fe−C−H = Fe−C−C = 120°. Modeling the S−CH=CH$_2$ moiety required no extra parameters. All force constants were set to an arbitrary value of 80% of the values for sp^3 C−C and C−C−C bond lengths and angles, respectively. Chem-X geometry optimizations on FeMoco and its local protein environment were carried out keeping all FeMoco atoms, apart from the FeS_3 moiety involved in substrate binding, and all protein backbone C and N atoms as a fixed restraint.

Insight II calculations were performed on the α-subunit of crystal structure 1M1N (*6*), using the Discover module and cvff force field. During geometry optimizations, all atoms of protein residues 4−62 and 241−480 were kept fixed, while for residues 79−240 only the backbone atoms were fixed. Residues 63−78 were fully unconstrained. The -CH=CH$_2$ group, FeMoco core cluster, and homocitrate were fixed, and partial atomic charges were specified based on the output from the DFT calculations; the P-cluster was omitted. The geometry optimization of the propargyl alcohol reduction intermediate was done in the same way, except that the side chain of residue 279 was also allowed to move. The output structures were validated within Insight II using Procheck.

All DFT calculations were performed using the B3LYP functional and LanL2DZ basis set as implemented in GAUSSIAN 98W (*41*). Geometry optimizations were carried out using partial z-matrix methods on all spin states considered possible allowing for both ferromagnetic and antiferromagnetic coupling of the metal spins. In general, the default convergence criteria proved unsatisfactory; after an initial phase in which the energy fell rapidly on each step, there followed a large number of steps in which the energy changed insignificantly. Therefore, geometry optimization was terminated when the change in energy was less than 0.1 kcal mol^{-1} over 10 consecutive optimization minima. For the [S_2FeSFeS_2]-based fragments, dummy atoms X were employed such that all three X−Fe−S angles were kept coequal, and the $S_{terminal}$−Fe−X−$S_{bridging}$ dihedral angles were both fixed at 124.1°, the mean value from the Kp1 X-ray crystal structure. The Fe−S−Fe angle and all Fe−S distances were allowed to vary independently. For the [(HS)Fe(SH)$_2$Mo(SH)(OCH$_2$CO$_2$)] models, the metal−sulfur section was treated as having a plane of symmetry lying through the Fe and Mo atoms and the terminal SH groups, and the S−Mo−S angles were fixed at their experimental value of 102°. The glycolate ligand was allowed to refine freely. In the [Mo(SH)$_3$(OMe)(imH)] models, the S−Mo−S, O−Mo−S, and N−Mo−S angles were fixed at 102, 88, and 84°, respectively.

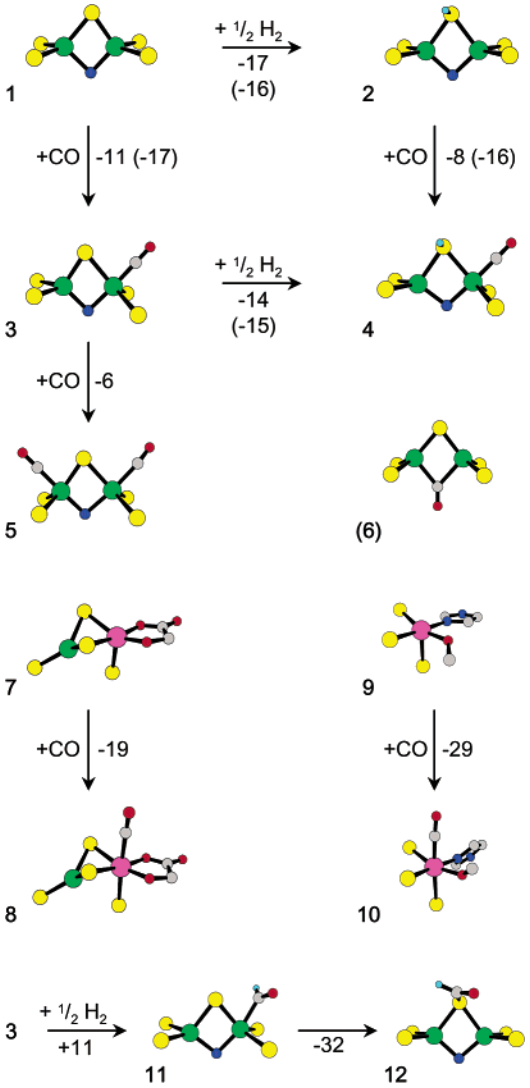

FIGURE 2: Geometry-optimized structures for CO binding to the $[(HS)(H_2S)Fe(S)(NH_2)Fe(SH)(SH_2)]$, $[(HS)Fe(SH)_2Mo(SH)(OCH_2CO_2)]$, and $[Mo(SH)_3(OMe)(imH)]$ model complexes. Color code: C, gray; H, pale blue; N, dark blue; O, red; Fe, green; Mo, purple, S, yellow. Note that structures **7**−**10** are anionic; all the others are neutral, but the structures change only slightly when carrying a charge. Hydrogen atoms not involved in reduction of the cluster or substrate are omitted for clarity. The formal oxidation states are as follows: **1**, **3**, **5**, $Fe^{3+}Fe^{2+}$; **2**, **4**, (**6**), **12**, $Fe^{2+}Fe^{2+}$; **7**$^-$, **8**$^-$, Fe^{2+}-Mo^{3+}; **9**$^-$, **10**$^-$, Mo^{3+}; **11**, $Fe^{3+}Fe^{3+}$.

Protein coordinates were retrieved from the Brookhaven Protein Data Bank (*42*), accession codes 1M1N (*6*) and 2MIN (*5*) (Av1) and 1QGU (*4*) (Kp1). Figures were prepared using Insight II (*40*) and ORTEP 3 for Windows (*43*).

RESULTS

Choice of Models for the DFT Calculations. Initially, the base model used to study the central Fe sites of the FeMoco consisted of a $[(HS)_2Fe(\mu\text{-}S)Fe(SH)(SH_2)]$ fragment. This gives formal oxidation states[2] of $Fe^{3+}Fe^{2+}$, in line with the characterization of the resting state enzyme as $[Fe^{3+}{}_3Fe^{2+}{}_4Mo^{4+}]$ (*9*, *10*, *13*, *14*). Addition of a hydrogen atom to the bridging sulfur reduces the model cluster to $Fe^{2+}{}_2$. However, during the course of this work, a new X-ray crystal structure revealed the presence of an additional light atom, most probably N, in the center of the FeMoco (*6*). The effects of this revision were allowed for by altering the base model to $[(HS)(H_2S)Fe(\mu\text{-}S)(\mu\text{-}NH_2)Fe(SH)(SH_2)]$ (Figure 2, **1**), which again has $Fe^{3+}Fe^{2+}$ oxidation states. In the following sections, structure numbers in parentheses relate to the original model, i.e., structures equivalent to those shown in Figures 2 and 3 but without the central NH_2 group. In general, the inclusion of the bridging NH_2 group made the Fe atoms rather less reactive toward all the ligands considered. This is not surprising given that these Fe atoms are no longer coordinatively unsaturated, as had been thought. Two models were used for the Mo site, namely, $[(HS)Fe(SH)_2Mo(SH)(OCH_2CO_2)]$ and $[Mo(SH)_3(OMe)(imH)]$, to model $[MoS_3O_2]$ and $[MoS_3ON]$ inner coordination spheres, respectively. Both of these models are formally Mo^{4+} when neutral, or Mo^{3+} when anionic. Since the Fe atom in the first model was included primarily to give the correct oxidation state at Mo, the omission of the N atom in this case should not significantly affect the chemistry of the Mo site.

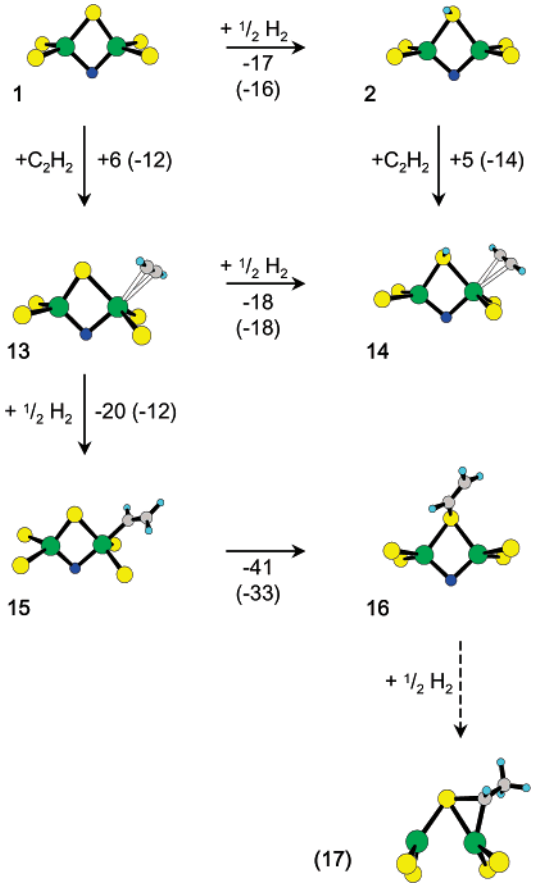

FIGURE 3: Geometry-optimized structures for C_2H_2 binding and reduction. The bonds to the C_2H_2 ligands in **13** and **14** are shown as open lines to indicate that the C_2H_2 dissociates in the absence of geometric constraints. Colors and other details as in Figure 2. The formal oxidation states are as follows: **13**, $Fe^{3+}Fe^{2+}$; **14**, **16**, $Fe^{2+}Fe^{2+}$; **15**, $Fe^{3+}Fe^{3+}$; (**17**), $Fe^{2+}Fe^{+}$.

DFT Calculations on CO Binding. Structure **1** and its reduced analogue **2** (Figure 2) can both accept a CO ligand, bound in the classical end-on fashion, to give **3** and **4**, with CO binding energies of −11 and −8 kcal mol^{-1}, respectively. The slightly lower binding energy for **4** compared to **3**

[2] Note that throughout this paper, oxidation states are written as localized on individual metals; however, this formalism should not be taken to imply that valence electrons are necessarily so localized.

suggests that it is harder to add a hydrogen atom to the cluster when CO is bound; the energies for hydrogen atom addition, calculated with respect to $1/2H_2$ as a reference state, are −17 and −14 kcal mol^{-1} for **1** and **3**, respectively. Hydrogen atom addition is a composite process, involving both reduction and protonation. Calculations on the corresponding anions $\mathbf{1}^-$ and $\mathbf{3}^-$ indicate that it is the protonation step that is primarily responsible for the difference in energies, being 4 kcal mol^{-1} less favorable for $\mathbf{3}^-$ than for $\mathbf{1}^-$. Although these small differences should be treated with caution, since the current calculations neglect protein environmental effects, they are consistent with experiment. Thus, CO binding appears to make the isolated FeMoco easier to reduce (*14*, *35*), but also renders the FeMoco less basic, evidenced by the observed shift of an FeMoco-associated p*K* from ∼9 to ∼8.5 in the presence of CO (*44*). This is also the normal reactivity pattern that would be expected based on the extensive literature for simple CO complexes. The central nitrogen atom weakens CO binding; the equivalent binding energies for the model without a central NH_2 group are −17 and −16 kcal mol^{-1} for **3** and **4**, respectively. A second CO ligand can be added to **3** yielding **5**; however, the second CO binds more weakly. Note that none of the models considered in this study was capable of binding more than one CO ligand at each individual metal site.

In view of suggestions based on ENDOR spectroscopic data (*45*) that CO binds to the central Fe atoms of the FeMoco in a bridging mode, this possibility was also considered in some detail. However, modification of the Fe−C≡O moiety in **3** toward a more bridging geometry was accompanied by significant energy penalties; the CO binding energy decreases rapidly as the Fe−C≡O bond angle moves away from 180°, reaching a value of 0 for an Fe−C≡O angle of 148°. MM modeling on the whole FeMoco suggested that CO bridging between adjacent central Fe atoms might be possible by means of a distortion of the cluster such that one of the central S atoms is displaced out of the Fe_2N plane (where N is the central atom within the FeMoco). This possibility was tested by DFT calculations on a modified form of structure **3**, in which the central S atom was displaced in this fashion, and the CO ligand was placed in a bridging position between the two Fe atoms. However, on geometry optimization, the structure reverted to that of **3** for the ferromagnetically coupled spin states, and the CO ligand dissociated completely from the cluster for the antiferromagnetic spin state. In view of this failure to locate even a metastable bridging CO structure for the base model, an additional, "ideal" CO bridging structure was also considered, in which the NH_2 ligand was replaced by CO [Figure 2, (**6**)]. It is important to note that FeMoco itself would not be able to attain such a geometry; nevertheless, it should be superior to any CO-bridged geometry which FeMoco could actually achieve, since it invokes the now-discredited three coordinate irons. The lowest energy spin state for (**6**) was calculated to be the ferromagnetically coupled, $S = 9/2$ state; however, after geometry optimization, the CO had taken up a nonbridging, end-on coordination mode on one Fe atom only (the bonded and nonbonded Fe−C distances were 2.13 and 3.71 Å, respectively). Structure (**6**) in Figure 2 is, in fact, that of the antiferromagnetically coupled $S = 1/2$ spin state, with Fe−C distances of 2.19 and 2.27 Å; however, this state was 6 kcal mol^{-1} higher in energy than the ground state, with a CO binding energy of −7 kcal mol^{-1}, inferior to that of the simple, end-on bound structure **3** discussed above. Very similar results were obtained when starting from a $\mu-\eta-$CO geometry similar to (**6**) but with the CO group angled to make an initial bonding Fe−O contact. Table 1 lists the calculated CO frequencies for the structures shown in Figure 2. The primary determinant of ν(CO) is the charge on the complex, with $\mathbf{3}^+$, $\mathbf{3}^0$, and $\mathbf{3}^-$ giving progressively lower ν(CO) brackets. Spin state has a smaller effect, modulating ν(CO) over a range of ∼30 cm^{-1} for a given charge state. The oxidation states of the metals appear to have little influence; for example, the $Fe^{3+}Fe^{2+}$ species **3** has an almost identical ν(CO) range to that of the $Fe^{2+}Fe^{2+}$ species **4**.

Table 1: Calculated CO Frequencies for the Species Shown in Figure 2

structure	ν(CO)[a], cm^{-1}	structure	ν(CO), cm^{-1}
$\mathbf{3}^+$	2055−2080 (2063)	(**6**)	1929−2022 (2022)[b]
3	1985−2016 (1985)	**8**	1977−2038 (1977)
$\mathbf{3}^-$	1907−1932 (1932)	$\mathbf{8}^-$	1903−1961 (1961)
4	1985−2010 (1985)	$\mathbf{10}^-$	1819−1892 (1819)
5	1999−2001 (2001), 2009−2022 (2022)	**12**	1644−1649 (1649)
$\mathbf{5}^-$	1912−1930 (1912), 1937−1948 (1939)		

[a] Range is for all spin states; value in parentheses is for ground spin state. [b] CO not bridging in the ground-state structure; bridging ν(CO) for $S = 1/2$ structure is 1963 cm^{-1}.

A final important aspect of CO binding at the Fe sites is the effect on the spin state of the metal. In the absence of CO, the ground state is antiferromagnetically coupled and the calculated spins on both Fe atoms are relatively invariant at ±(3.5−3.7), regardless of the formal Fe oxidation states or the overall spin state of the complex, with the residual spin largely on the sulfurs. This holds true for **1**, $\mathbf{1}^+$, $\mathbf{1}^-$, and **2**. However, for the CO complexes **3**, $\mathbf{3}^+$, $\mathbf{3}^-$, and **4**, the ground state structures are ferromagnetically coupled, with a spin of 2.1−2.6 on the Fe atom bound to CO. The ground states for the dicarbonyl complexes **5** and $\mathbf{5}^-$ revert to antiferromagnetic coupling, with one low spin and one high spin Fe [spins of −(2.1−2.6) and +3.5, respectively]. The switch from high- to low-spin on coordination of CO is in agreement with experimental results for the complex $[Fe(CO)(NS3)]^-$ [$NS3 = N(CH_2CH_2S)_3^{3-}$], which was found to be low spin, in contrast to $[FeX(NS3)]^-$ (X = Cl or N_3), which were both high spin (*46*).

The Mo atom was also considered as a potential binding site for CO, a possibility that would most likely require the loss of one ligating atom from its coordination sphere, since the geometry around Mo appears poorly suited for seven coordination. When FeMoco is extracted from the protein, the histidine ligation to Mo must be lost, but it appears that the homocitrate ligand is retained (*47*). The coordination sphere of the Mo in this case would then be $[MoS_3O_2]$, which was modeled using the structure shown in Figure 2, **7**. With respect to intact, functioning nitrogenase, it has been postulated that the Mo atom may become five-coordinate during catalysis via opening of the homocitrate chelate ring (*37*, *47*), in which case the Mo atom would attain a [MoS_3-ON] coordination sphere, modeled as in Figure 2, **9**. The two anions $\mathbf{7}^-$ and $\mathbf{9}^-$ both bind CO more strongly than do the Fe sites discussed above; moreover, they have markedly

different CO binding energies, of −19 and −29 kcal mol^{-1}, respectively. The calculated ν(CO) frequencies for the [MoS_3O_2(CO)] structures **8** and **8**$^-$ vary somewhat with the overall spin state, and are similar to those for the iron-based fragments discussed above, while ν(CO) for the [MoS_3ON(CO)] fragment **10**$^-$ varies by 73 cm^{-1} depending on the spin state; the ground state, low spin ($S = 1/2$) structure has the lowest carbon monoxide frequency found in this work, at 1819 cm^{-1}.

The possibility of reduction of CO to formaldehyde by a mechanism similar to that proposed below for C_2H_2 was considered. Thus, reduction of **3** could in principle be associated with protonation at sulfur to give **4**, or at the CO ligand to give the thioformate species **12**. The second possibility gives the thermodynamically preferred product, i.e., **12** is 6 kcal mol^{-1} more stable than **4**. However, **12** would have to be produced via an initial Fe−CH═O intermediate, **11**, which is 25 kcal mol^{-1} higher in energy than **4**. Hence, reduction of CO to formaldehyde by nitrogenase appears to be thermodynamically favorable but kinetically unfavorable.

DFT Calculations on Acetylene Binding and Reduction. Initial calculations were carried out on the model lacking a central Fe atom; selected calculations were subsequently repeated for the N-containing model, with similar results. The results are summarized in Figure 3. As observed for CO, the presence of the central N atom serves to weaken C_2H_2 binding at Fe; however, the effect is somewhat larger for C_2H_2 and binding is endothermic for both **13** and **14** (+6 and +5 kcal mol^{-1}, respectively). In fact, to prevent dissociation of the C_2H_2 during geometry optimization it was necessary to build in additional geometric constraints (the distance between the Fe and the centroid of the C≡C bond was fixed at 2.55 Å). Thus, initial binding of C_2H_2 to a single Fe site is characterized as a loose association only. In line with this, the energetics of hydrogen atom addition to the central S are essentially unperturbed by the presence of a C_2H_2 ligand on Fe. However, the hydrogen atom can also now be added to the C_2H_2 ligand rather than to S, with very similar energy; formal addition of 1/2H_2 to the C_2H_2 ligand in **13** to give the vinylidene species **15** has an energy of −20 kcal mol^{-1}, compared to −18 kcal mol^{-1} for addition to the central S to give **14**. Most interestingly, the Fe-bound species **15** is highly unstable with respect to transfer of the vinyl group to S, giving species **16**. This reaction appears to be both thermodynamically and kinetically favored; for the equivalent model lacking the central NH_2 group (**15**), transfer of the -CH═CH_2 group from Fe to S occurred spontaneously during the geometry optimization for some spin states. This suggests that there is essentially no kinetic barrier to the rearrangement. In these cases, the output geometry retained a coordinate bond between Fe and the vinyl group's π-bond in addition to the new C−S bond; although slightly higher in energy than the geometry where the coordinate bond has been lost, (i.e., **16**), this indicates the probable reason for the low energy barrier for the rearrangement.

A final point of interest for the reactions of C_2H_2, studied using the original model, concerns the fact that there are two possible sites for hydrogen atom addition to the S−CH═CH_2 moiety, namely, the α- or β-carbon atoms. Addition to the α-carbon gives C_2H_4, which can then be released from the cluster. However, addition to the β-carbon gives a -$CHCH_3$ ligand, which takes up a bridging position between S and Fe [Figure 3, (**17**)]. This is only 5 kcal mol^{-1} higher in energy than the first alternative. Since further reduction of (**17**) would give C_2H_6, this suggests a secondary reduction pathway for C_2H_2 to give C_2H_6 rather than C_2H_4; note however that C_2H_4 itself cannot give (**17**) without undergoing C−H bond cleavage, which is likely to be a high energy process.

The set of calculations described above for C_2H_2 were also carried out for C_2H_4 using the original model. The energies of all the reactions were very similar, with one significant exception; the energy for transfer of a hydrogen atom from the central S to C_2H_4 to give the Fe−CH_2CH_3 complex was +16 kcal mol^{-1}, compared to +6 kcal mol^{-1} for the equivalent reaction in the C_2H_2 system [i.e., conversion of (**14**) into (**15**)]. The possibility of C_2H_4 reduction on Mo was also considered, using the homocitrate ring-opened model site **9** (Figure 2). The calculated C_2H_4 binding energy was −3 kcal mol^{-1}, and the energy for transfer of a hydrogen atom from the central S of species **2** to the Mo-bound substrate was +9 kcal mol^{-1}, rather better than the value for the Fe site noted above. However, the Fe-based species can relax via transfer of the -CH_2CH_3 group to S, but this possibility is not open to the Mo site. Therefore, the Mo site should be even less competent for reduction of C_2H_4 than is the Fe site.

MM Calculations. Previously, the ability of each of the six central Fe atoms of the FeMoco to accommodate a terminally bound N_2 ligand was analyzed in terms of the degree of van der Waals overlap with the surrounding protein (*37*). Given that CO complexes are geometrically very similar to their N_2 counterparts, this analysis should also be valid for terminal CO binding. Hence, it may be concluded that Fe2, Fe3, Fe5, Fe6, and Fe7 can all accommodate a terminally bound CO with only minor perturbations of the surrounding protein.

In the present work, this analysis has been extended to consider acetylene and the possible intermediates in its reduction. The three species considered were side-on bound C_2H_2 and the first reduction intermediate, bound either to iron (Fe−CH═CH_2) or sulfur (S−CH═CH_2). The optimized geometries from the DFT calculations were used to construct the appropriate ligands on the FeMoco, and the degree of van der Waals overlap with neighboring protein residues was measured before and after MM optimization of the protein side chains, keeping the portion of FeMoco not involved in ligand binding plus the protein backbone atoms as a fixed constraint. The results are given in Table 2; the abilities of the Fe sites to accommodate both C_2H_2 and -CH═CH_2 ligands are very similar to those found previously for N_2. Only Fe4 is clearly ruled out as a potential binding site. Placing the -CH═CH_2 group on each of the three central sulfurs of the FeMoco gives two possible stereoisomers; these are labeled as *a* and *c* in Table 2, indicating that the -CH═CH_2 group is disposed anticlockwise or clockwise when viewing the FeMoco from the Mo toward the terminal Fe. For all six isomers, significant steric hindrance with the surrounding protein is observed before geometry optimization. Relaxing the protein side chains relieves these contacts for the *c* orientations of both S3A and S5, but not for S2B. Interestingly, however, one of the principal residues responsible for the steric congestion at S2B is α-Val^{70}. Mutations

Table 2: Degree of van der Waals Overlap (%)[a] between C_2H_2 and -CH═CH_2 Groups Attached to the Central Fe and S Atoms of FeMoco and the Surrounding Protein[b]

Fe atom	adjacent S atom	Fe−C_2H_2 overlap raw[d]	Fe−C_2H_2 overlap opt[e]	Fe−CH═CH_2 overlap raw	Fe−CH═CH_2 overlap opt	S−CH═CH_2 overlap (*c* orientation)[c] raw	S−CH═CH_2 overlap (*c* orientation)[c] opt	S−CH═CH_2 overlap (*a* orientation) raw	S−CH═CH_2 overlap (*a* orientation) opt
Fe2	S2B (1)[f]	18	2	22	4	36	*g,h*	37	*g*
Fe6	S2B (1)	4	1	5	0				
Fe3	S5 (2)	13	0	7	0	17	1	49	*g*
Fe7	S5 (2)	4	1	2	2				
Fe4	S3A (−)	40	*g*			36	1	43	*g*
Fe5	S3A (−)	14	4	7	3				

[a] Data calculated using the Kp1 crystal structure. [b] Expressed as percentage of van der Waals volume of free C_2H_2 or -CH═CH_2 as appropriate (28.3 and 29.9 Å^3, respectively). [c] *c* and *a* denote clockwise and anticlockwise orientations respectively for the S−CH═CH_2 moiety when viewed down the long axis of the MoFe cluster, with the Mo atom projecting toward the viewer. [d] Before geometry optimization. [e] After geometry optimization. [f] Numbers in parentheses give the predicted order of protonation of the sulfurs in the wild-type protein; S3A has no proton delivery channel. [g] Failed to give a satisfactory energy-minimized structure in geometry optimizations keeping all protein backbone atoms fixed. [h] Vinyl group can be accommodated by movements in the protein backbone; see text.

in this residue and in α-Gly^{69} are known to have an important influence on the characteristics of C_2H_2 reduction by Av1 (*24*, *31*, *32*). To test whether an S−CH═CH_2 intermediate could provide an explanation of these experimental observations, the conformational analysis was extended to consider the possibility of movement in the backbone of this region of the protein.

As already pointed out by Dean and co-workers (*24*, *31*), α-Gly^{69} and α-Val^{70} are part of a short helix running between FeMoco and the P-cluster. It proved possible to resolve the steric clash between α-Val^{70} and the S−CH═CH_2 group by means of geometry optimization on this region of the protein structure, centered on residues 63−78 of the α-subunit. Residue α-Cys^{62} is a ligand to the P-cluster; hence, this forms an obvious fixed reference point, while residue α-Met^{78} marks the onset of a *β*-sheet region, which should be relatively rigid. Within the optimized region, the main movements were in residues 68−72; movement of the flanking residues was minimal. The output geometry for the wild-type protein with -CH═CH_2 bound at S2B, Figure 4, has no significant steric clashes and is geometrically valid. The large energy gain associated with transfer of the -CH═CH_2 group to S should provide ample driving force for this low energy movement within the protein. A more subtle question is why the substitution of α-Gly^{69} by Ser should prevent the acquisition of a -CH═CH_2 group by S2B. Introducing this point mutation into the model showed that α-Ser^{69} contacts the S−CH═CH_2 moiety; however, there were no steric clashes that could not be easily resolved. It seems more likely that the α-Ser^{69} mutation would somehow block formation of the initial Fe−CH═CH_2 intermediate, since this state is already the least accessible point on the reaction pathway. An interesting possibility is suggested by the observation that the α-Ser^{69} mutant side chain can form a hydrogen bond with atom O2 of the $CH_2CO_2^-$ carboxylate group of homocitrate when the helix incorporating α-Ser^{69} is in its modified geometry. The movement of the homocitrate -$CH_2CO_2^-$ arm required to form this hydrogen bond blocks Fe6 with respect to coordination of a -CH═CH_2 ligand. However, the movement does not disrupt the usual hydrogen bond between atom O1 of the homocitrate and residue α-Gln^{191}; in fact, it is similar to the movement postulated for maintaining this hydrogen bond in the homocitrate ring-opened, N_2-bound state modeled previously (*47*). Hence, this model study suggests how the α-Ser^{69} mutation could block the primary route for C_2H_2 reduction but leave N_2 reduction unperturbed, in line with the experimental observations (*24*). It was also possible to use this backbone movement to model the corresponding intermediate for reduction of propargyl alcohol, i.e. *trans*-S−CH═$CHCH_2OH$, provided that α-Val^{70} was replaced by Ala. In this case, the -OH group of the partially reduced substrate can form an adventitious hydrogen bond with S2A of the FeMoco (Figure 5).

DISCUSSION

CO Binding. Extensive spectroscopic studies on CO binding to the FeMoco, both in the functioning protein and in protein-free extracts, have been interpreted in terms of combinations of two CO distinct binding modes, namely, terminal binding to a single metal center, and bridging to two adjacent metals (*14*, *30*, *45*, *48*−*50*). The results of the present study are in good agreement with the first of these models, i.e., terminal binding of CO to single Fe sites. The *ν*(CO) for the ground state of the anion **3**$^-$, at 1932 cm^{-1}, is very close to that calculated for the complex anion [Fe(CO)(NS3)]$^-$, using exactly the same method, of 1926 cm^{-1}. This complex shares the same Fe inner coordination sphere and geometry as the central Fe atoms of the FeMoco. The experimental value for this complex is 1885−1910 cm^{-1} depending on the sample conditions, while the related neutral complex [Fe{Fe(CO)(NS3)}$_2$] gave an experimental *ν*(CO) range of 1937−1961 cm^{-1} (*46*).[3] Hence, the bands observed in SF-FTIR experiments on functioning nitrogenase, at 1880, 1904, 1936, and 1958 cm^{-1} can all be reasonably assigned to terminal CO, most likely bound to a neutral or anionic FeMoco core. The exact position of the CO frequency will be modulated by the charge and spin state of the cluster as well as the number of CO ligands and environmental effects from the protein. With respect to the second proposed CO binding mode, however, no indication of a stable bridging CO structure has been found in the DFT calculations on FeMoco fragments presented above. This appears to be due to steric repulsion from the central sulfur atoms of the FeMoco when CO is placed in a bridging position between two iron atoms, together with the rather weak CO binding energy found in the calculations. Attempts to model a bridging CO on whole FeMoco by MM, in the manner suggested in the literature (*14*, *45*), suggest that such a binding mode would require a distortion of the FeMoco involving movement of the central S atoms. However, the DFT calculations indicate that the energies required for such distortions more than offset the gains from CO binding. It could be argued that the FeMoco undergoes a more drastic

[3] Infrared frequencies calculated by quantum methods are in general slightly overestimated due to systematic errors; the values reported in this paper are uncorrected for these effects, but the comparison between observed and calculated *ν*(CO) values for [Fe(CO)(NS3)]$^-$ indicates that the resulting uncertainty, together with environmental effects, probably amounts to ∼20−50 cm^{-1}.

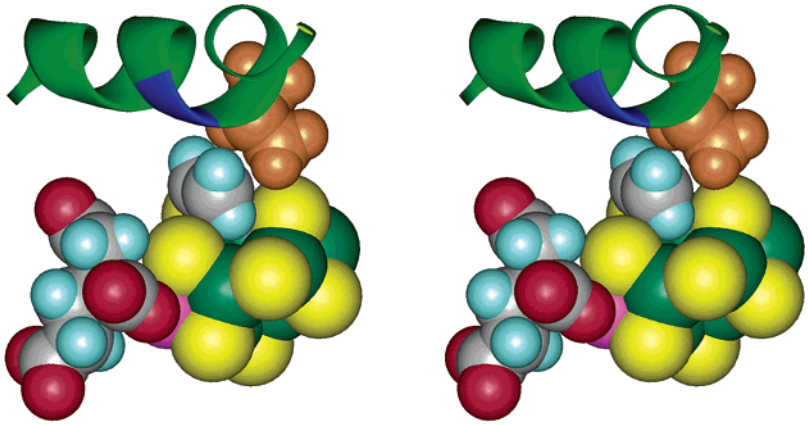

FIGURE 4: Wall-eyed stereoview of FeMoco with a -CH═CH_2 group bound at S2B, after geometry optimization (see text). The short helix from the α-subunit, residues 62−76, is shown in ribbon format, with the side chain of α-Val^{70} in spacefilling mode (orange). The position of α-Gly^{69} is shown in blue; atom colors as in Figure 2.

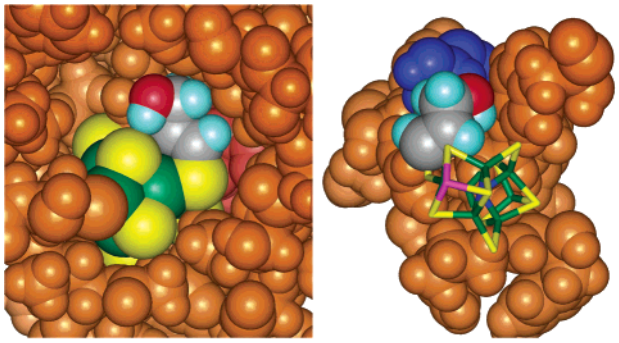

FIGURE 5: Spacefilling view of the putative S−CH═$CHCH_2OH$ intermediate for the reduction of propargyl alcohol by the α-Ala^{70} mutant. (a) View of protein residues within 10 Å of the FeMoco, with selected residues hidden to reveal the -CH═$CHCH_2OH$ group. The homocitrate is colored pink. (b) View of those residues which were hidden in panel a, viewed from the opposite side of the FeMoco. Residue α-Ala^{70} is shown in blue and the FeMoco is rendered as sticks for clarity. Atom colors as in Figure 2.

distortion to accommodate a bridging CO ligand, but there is at present no experimental evidence for gross structural changes in the FeMoco on CO binding. By definition, any distortion of the FeMoco will also have an attendant energy cost that will rapidly offset the moderate energy gain from CO binding as the extent of the distortion increases. The essential problem for envisaging bridging of CO, or indeed of any other ligand, on FeMoco is that the outer surface of the FeMoco is dominated by sulfur atoms (*6*), whose nearest neighbor separations, at 3.8−3.95 Å, are already close to the sums of their van der Waals radii.

Another conceivable way for CO to bridge between two metals in the FeMoco would be between an Fe atom and the Mo atom, once a vacant coordination site had been made available at the latter. Earlier calculations suggested that both NNH^- (*37*) and CN^- (*51*) form bridging interactions with the neighboring Fe atom when bound at Mo. However, geometry optimization starting from a bridging CO in complex $\mathbf{8}^-$ also gave a terminally bound CO, as shown in Figure 2, with no hint of a stable bridging mode.

Two major lines of experimental evidence have been used in support of the proposed bridging CO structure. First, $^{13}C/^{1}H$ ENDOR spectra of functioning nitrogenase under low CO pressures were interpreted in terms of a bridging CO ligand (*45*). An alternative explanation for the observed spectroscopic features, namely, CO terminally bound to a single, low-spin Fe, was also considered, but rejected as lacking experimental precedents. It is interesting that the calculations reported herein tend to support this alternative explanation, in that binding of a single CO does indeed cause a change from high-spin to low-spin at the Fe atom. The second source of experimental data suggesting a possible bridged CO comes from SF-FTIR studies. The lowest CO frequency reported in the original SF-FTIR paper (*30*) was 1904 cm^{-1}. Although George et al. interpreted this as typical of terminally bound CO, Lee et al. pointed out that this band might also arise from a bridging CO (*45*). As discussed above, experimental studies on model complexes and the theoretical results presented in this study both strongly support the view that the 1904 cm^{-1} band arises from CO terminally bound to a single Fe center. The CO frequency for the "ideal" CO-bridged cluster (**6**) is rather higher, at 1963 cm^{-1}; moreover, as noted above, this structure is unstable with respect to reversion of the CO to a terminally bound geometry.

Later SF-FTIR studies on whole nitrogenase identified an additional CO-derived band at 1715 cm^{-1} (*49*). This is much closer to the expected region for a bridging CO ligand; however, it appears relatively slowly over a time scale of several minutes, suggesting that it may constitute a slowly formed but thermodynamically stable product state. Given the slow time scale involved in its appearance it is unlikely to be associated with the species assigned to bridging CO in the ENDOR experiments. One possibility is that it involves protonation of the CO to give a -CH═O species. Formaldehyde itself appears at 1660−1730 cm^{-1} in a range of organic solvents (*52*). It may be that CO can be slowly reduced by a pathway analogous to that for acetylene, see below, with either a thioformate derivative of FeMoco or free formaldehyde as the final product. The thioformate complex **12** in Figure 2 has a CO frequency of 1649 cm^{-1}, rather lower than the experimental frequency. Although formation of **12** is thermodynamically favorable with respect to addition of hydrogen at the sulfur, the relative instability of the required intermediate **11** should make this process kinetically unfavorable. This would be consistent with the slow development of the 1715 cm^{-1} band.

A final consideration in this section is the experimental data obtained for CO binding to extracted FeMoco on reduction (*14*, *35*). In these experiments, a number of bands were observed between 1885 and 1930 cm^{-1} upon reducing the isolated FeMoco under CO. These are in a similar region to the bands observed for whole nitrogenase by SF-FTIR, and were assigned to terminally bound CO. However, two additional, very weak bands were observed at 1808 and 1835 cm^{-1} at low CO concentrations, and assigned to bridging CO (*14*). In the present calculations, the only bands falling in this region arise from the model for the Mo site with imidazole bound and monodentate homocitrate, $\mathbf{10}^-$ (Table 1). However, this is unlikely to explain the experimental observations since (i) the FeMoco preparations giving rise to these bands did not contain imidazole, and (ii) the associated electrochemistry suggested that these bands are associated with the central Fe atoms rather than Mo. It is perhaps significant that no bands were found in this region in the SF-FTIR studies on whole nitrogenase. Given the problems noted above for *intramolecular* CO bridging, another possible assignment for these bands is to *intermolecular* CO bridging in solutions of FeMoco, i.e., $[FeMoco]_2$-(CO). Such linearly bridging CO ligands show a very wide range of infrared frequencies, depending on the strength of the bridging interaction, which at the higher end encompass the values mentioned above. For example, the complex $[\{Fe(CO)_3(\mu\text{-}CO)\}Sn\{Fe(C_5H_5)(CO)_2\}_2]_2$ (*53*), which contains an Fe−CO−Sn moiety, has a bridging CO frequency of 1824 cm^{-1}. Molecular modeling suggests that Fe−CO−Fe bridging between two molecules of FeMoco is sterically feasible.

To summarize, most of the experimentally observed infrared bands can be assigned to CO terminally bound to single central Fe atoms of the FeMoco. The observation of different bands at higher CO concentrations is assigned to coordination of more than one CO to the same FeMoco, together with differences in the protonation state and charge of the cluster and local environmental effects. The bands below 1880 cm^{-1} can be plausibly assigned to intermolecularly bridged CO in the electrochemical studies and to a C═O species, possibly formaldehyde, in the SF-FTIR studies. None of the observed infrared bands necessitate the postulation of an intramolecularly bridging CO ligand.

The noninvolvement of the Mo atom of nitrogenase in CO binding implied in this work is consistent with the Mo-based model for N_2 proposed earlier (*37*). In that model, Mo only becomes available for coordination of N_2, and by extension CO, at redox level E_3, via opening of the homocitrate chelate ring, while electrochemical studies on isolated FeMoco (*14*) indicated that redox states equivalent to E_1 and E_2 are primarily responsible for CO binding. It should be noted that in extracted FeMoco, the Mo site may be available earlier than E_3, since the cofactor has lost its imidazole ligand. However, the calculated ν(CO) ranges for CO bound to a $[MoS_3O_2]$ site, resulting from loss of imidazole, are markedly higher than those for CO bound to a $[MoS_3ON]$ site, resulting from homocitrate ring opening, and cover essentially the same range as CO bound to the Fe sites (cf. $\mathbf{8}^{0/-}$ and $\mathbf{3}^{0/-}$ in Table 1).

Acetylene Binding and Reduction. According to the DFT calculations, initial binding of C_2H_2 at the central Fe sites of the FeMoco is very weak. As with CO, it has been proposed that C_2H_2 might bridge between two or more of the central Fe atoms of the FeMoco. However, the steric clashes encountered when attempting to model this possibility are even more severe than those for CO, and no such bridging mode could be plausibly modeled in the course of the present study. At first sight, this observation is at odds with experimental studies that clearly indicate the importance of the central Fe_4S_4 "faces" of the FeMoco in acetylene reduction (*24*, *31*, *32*). However, an alternative explanation for the experimental observations is provided by the predicted course of C_2H_2 reduction on FeMoco, as follows. Even though initial binding of C_2H_2 is very weak, the calculations indicate that a C_2H_2 ligand can successfully compete with the central S atoms of FeMoco for incoming protons. The initially formed Fe−CH═CH_2 intermediate is unstable with respect to spontaneous transfer of the vinyl group to the central S atom of the FeMoco. Experimentally, this kind of chemistry is now well established; for example, Rakowski Dubois and co-workers have described several systems in which the reduction of alkynes to alkenes on metal−sulfur clusters proceeds via intermediates containing carbon−sulfur bonds (*54*). More recently, tungsten−sulfur complexes containing bridging S−CH═CH_2 groups, with a single carbon−sulfur bond, have been prepared by reaction of the precursor complexes with C_2H_2, and characterized by X-ray crystallography (*55*, *56*). Note that although doubly bridging acetylene adducts, S−CH═CH−S, are often formed in such systems, this possibility is unlikely for FeMoco because its central S atoms are significantly further apart than in the smaller synthetic clusters.

The steric properties of the resulting S−CH═CH_2 species are very similar to those that would be expected for C_2H_2 bound to an Fe_4S_4 "face" of the FeMoco, and offer an alternative explanation for the experimentally proven significance of α-Gly^{69} and α-Val^{70} in C_2H_2 reduction. Specifically, accommodation of the vinyl group on S2B of FeMoco introduces a steric clash with α-Val^{70}, which can be relieved either by mutation of α-Val^{70} to alanine or by an internal rotation in the short helix of which α-Val^{70} is a member. Very recently, it has been reported that the α-Ala^{70} mutant reduces both propyne and propargyl alcohol (HC≡CCH_2-OH), and that in the last case an intermediate in the reduction can observed by EPR (*32*). It was suggested that the hydroxyl group of propargyl alcohol might stabilize the intermediate by an interaction with the protein. Modeling a -CH═$CHCH_2$-OH intermediate onto S2B indicates first that there is sufficient space to accommodate this group in the α-Ala^{70} mutant (but not the wild type), and second that the OH group of the intermediate is well placed to form a hydrogen bond with S2A of the FeMoco (Figure 5).

The assignment of the primary site for the S−CH═CH_2 intermediate to S2B raises an interesting question when compared with the analysis of steric hindrance around the three central S atoms, Table 2. This suggests that all three sulfurs could accommodate a vinyl group. Clearly, if this analysis is correct, then some other factor apart from steric constraints must determine the rates of formation of vinyl intermediates at the three central sulfur atoms. A plausible candidate is the relative rates of protonation of the sulfurs during nitrogenase turnover. Thus, a previous analysis of the protein (*36*) identified proton delivery channels to both S2B and S5 but not to S3A; furthermore, the channels appear to be constructed such that S2B should be protonated before

S5 during turnover. It was suggested that spontaneous migration of hydrogen atoms from the central S atoms to neighboring Fe atoms could be responsible for the experimentally observed loss of H_2 from states $E_2 - E_4$ in the Lowe-Thorneley scheme. Extending this argument to the reduction of acetylene, rearrangement of a proton from S2B or S5 to a neighboring Fe carrying a C_2H_2 ligand would allow the formation of a vinyl ligand on that Fe, which would then spontaneously migrate to the same sulfur.[4] (*57*)

It has long been recognized that nitrogenase has two types of C_2H_2 binding site with significantly different K_m values (*58*, *59*). The effects of the Av1 α-Gly^{69} mutation were interpreted in terms of elimination of the high affinity C_2H_2 binding site on the Fe_4S_4 "face" of the FeMoco associated with α-Val^{70}, while leaving the second, low affinity C_2H_2 binding site essentially unperturbed (*24*). In the present model, the two different K_m values can be interpreted in terms of reduction of C_2H_2 via S−CH═CH_2 intermediates formed on both S2B and S5, but with a higher rate of formation on S2B, due to the more favorable transfer of a proton to S2B compared to S5 for the electronic and structural reasons discussed previously (*36*). Steric hindrance of S−CH═CH_2 formation on the S2B site then results in an apparent loss of the high affinity C_2H_2 site.

Although the effects of the α-Gly^{69} and α-Val^{70} mutations can be assigned primarily to steric effects, other mutants may give rise to electronic effects. These can be further divided into mutants in which the effect lies with proton transfer to FeMoco and/or substrate, and those in which electron transfer to FeMoco is perturbed. Examples of both types can be deduced from the literature. For example, an Av1 mutant in which α-Arg^{277} was replaced by His showed sigmoidal kinetics for C_2H_2 reduction under nonsaturating levels of CO, indicative of two distinct C_2H_2 reduction sites and a third site for simultaneous binding of CO (*25*). As previously discussed (*36*), the α-His^{277} mutation is likely to reduce (but not completely eliminate) the efficiency of proton delivery to S2B of the cofactor. Under these circumstances, the normally efficient route for C_2H_2 reduction via S2B would be degraded, while the lower efficiency path via S5 would be unaffected. Initial binding of C_2H_2 and protonation to the Fe−CH═CH_2 intermediate would occur at the Fe sites adjacent to S2B and S5, i.e., Fe2, Fe3, Fe6, and Fe7 (cf. Table 2), while CO inhibition would result from simultaneous binding of CO at one of these four sites.

Another interesting set of Av mutants have substitutions of the wild-type residue α-His^{195} (*16*, *18*, *27*). There is a progressive lowering of specific activity for C_2H_2 reduction by the MoFe protein in going from the wild type (100% activity) through the α-Gln^{195} mutant (68%) to the α-Asn^{195} mutant (8%) (*16*). The wild-type α-His^{195} residue is hydrogen bonded to S2B of the cofactor and is part of a putative proton relay to that atom (*36*), while the α-Gln^{195} mutant retains a hydrogen bond to S2B (*27*), but is unable to relay a proton, and the α-Asn^{195} mutant presumably lacks even the ability to hydrogen bond to S2B (*36*, *60*). These observations suggest that the rate of C_2H_2 reduction is correlated to the electronic condition of the cofactor. Thus, in the wild-type protein, reduction of the cofactor is facilitated by transfer of a proton from α-His^{195} to S2B, whereas the α-Gln^{195} mutant can only partially compensate for the extra charge by means of a hydrogen bond to S2B, and the α-Asn^{195} mutant lacks even this capability. EPR studies of C_2H_2 reduction by the α-Gln^{195} mutant revealed three new signals, not observed for the wild-type nitrogenase (*26*, *27*). The first signal was assigned to simultaneous binding of C_2H_2 and partially reduced C_2H_x adducts to the FeMoco, while the second was consistent with the presence of an organic radical, possibly homocitrate. In the present model, these observations can be explained by a combination of two ideas. First, if the -CH═CH_2 group arrives at an S atom that either already carries a hydrogen atom or can receive one rapidly via a proton channel, the release of C_2H_4 should follow rapidly via proton transfer from S to C. The α-Gln^{195} mutant has lost its proton channel to S2B; hence, a -CH═CH_2 group in this position should be unusually long-lived. Second, spontaneous migration of -CH═CH_2 from Fe to S results in a reduction of the formal electron count of the metal centers of the FeMoco by two; this could leave the FeMoco in a highly reduced state not normally encountered in the wild-type catalytic cycle (see below), perhaps resulting in the formation of a radical anion on homocitrate.

Finally, it is noteworthy that the NifV$^-$ mutant nitrogenase, which has citrate in place of homocitrate, appears to reduce C_2H_2 normally (*61*, *62*); in vitro experiments on *K. pneumoniae* nitrogenase gave a K_m for acetylene reduction of 566 Pa, compared to 370 Pa for the wild type (*61*). In previous theoretical studies, the effects of substituting citrate for homocitrate on N_2 and H^+ reduction were interpreted in terms of substrate binding at Mo following opening of the (homo)-citrate chelate ring in states E_3 and beyond (*37*, *38*, *47*). In this context, the lack of a significant perturbation for C_2H_2 reduction is consistent with a process involving the Fe and S atoms of the FeMoco, but not the Mo.

Model for Acetylene Reduction. The reduction of C_2H_2 by nitrogenase from *K. pneumoniae* has been subjected to kinetic analysis, and a kinetic scheme for the reaction has been worked out (*21*, *22*). In this scheme, initial binding of C_2H_2 is assigned to state E_1, although additional binding at E_0 could not be excluded. Reduction of the C_2H_2-bound state beyond the E_2 redox level irreversibly commits the protein to C_2H_2 reduction, but C_2H_4 is not formed even on acid quench until the E_3 redox level is reached (*22*). Taking these observations together with the theoretical results presented above, an atomic level model for C_2H_2 reduction by nitrogenase can be proposed as in Scheme 1. This model is consistent with those previously proposed for the reduction of N_2 (*37*) and H^+ (*38*), with one modification, as follows. The earlier schemes predated the discovery of a central light atom within the FeMoco; hence, the oxidation state of the dithionite-reduced, resting state cluster core was taken as $[MoFe_7S_9]^+$. The consensus view from theoretical and experimental (*7*−*10*, *14*) studies published after the modification of the crystal structure is that the correct assignment is in fact $[MoFe_7NS_9]^0$. Starting from this oxidation level, a detailed assignment of the oxidation states for the intermediates in Scheme

[4] Note that although direct migration of a proton from S to Fe is the simplest possibility, a rearrangement involving two separate protons is probably more likely, i.e., the ability of the central Fe atoms to accept a proton from their surroundings is enhanced when the neighboring S atom is protonated. This is consistent with experimental studies which show that the addition of a proton to one of the η^2−S atoms in an $[Fe_3S_4]^0$ cluster controls the valence distribution of the three Fe atoms (*57*).

Scheme 1: Proposed Model for the Catalytic Reduction of Acetylene by Nitrogenase[a]

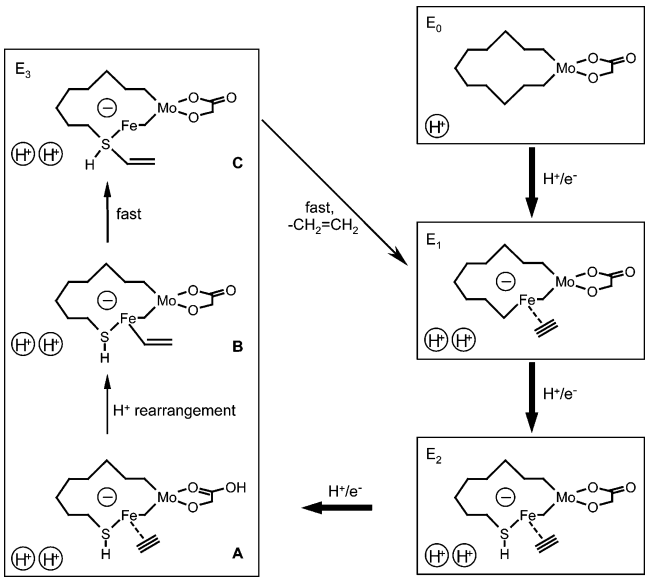

[a] For clarity, the FeMoco core cluster is shown schematically, and only the chelate ring of the homocitrate ligand has been included. The designations E_0, E_1, etc. refer to the Lowe-Fisher-Thorneley scheme (see ref *22*). Each of the bold arrows represents the transfer of a single e^- from the Fe protein to the MoFe protein. Circled H^+ represent nonlocated protons associated with the protein or homocitrate.

1 is given in Table 3. As in the previous models, each electron added to the system is associated with a proton transfer; in cases where the exact location of the proton cannot be deduced, these are designated with circles in Scheme 1.

It was previously suggested that the initial reduction of the resting state E_0 to E_1 results in a change in the charge on the core cluster rather than formal addition of a hydrogen atom, since E_1 releases H_2 much more slowly than the more reduced states (*37*). The revision of the core cluster assignment to $[MoFe_7NS_9]^0$ means that this charge increment will be from 0 to -1 rather than $+1$ to 0; this also fits in rather better with the ν(CO) data discussed above. Yoo et al. assigned this process to an Mo-based reduction, based on Mössbauer analysis of the MoFe protein under turnover conditions (*13*), and this is reflected in Table 3. It should be noted, however, that radiolytic reduction of the MoFe protein (*13*) and electrochemical reduction of isolated FeMoco (*14*) both appeared to give Fe-centered processes. The change in charge may be associated with the onset of detectable C_2H_2 binding for the wild-type protein. As with N_2, initial C_2H_2 binding is supposed to be weak and nonspecific, involving single Fe atoms; as shown in Table 2, up to five of the central Fe atoms may be involved in C_2H_2 binding and/or CO binding in the presence of CO. It should be noted that state E_0 may also bind C_2H_2, but even more weakly than the more reduced levels (*63*).[5] Further reduction gives state E_2, in which the incoming proton is assigned to S2B of the FeMoco, for the reasons discussed previously (*36*, *37*). The next state, E_3 **A**, is normally associated with addition of a proton to homocitrate. However, bound C_2H_2 can compete for this proton to give a transient Fe−CH=CH_2 intermediate, as in E_3, **B**. According to the DFT calculations, the barrier for transfer of the -CH=CH_2 group to S is essentially zero, so **B** will quickly rearrange to **C**. In the wild-type protein, state **C** should readily eliminate the product C_2H_4, so returning the system to E_1. However, the lifetime of state **C** can be increased by appropriate mutations; for example, the α-Gln^{195} mutant has no hydrogen atom on S2B, only a hydrogen bond to the side chain amide; hence, state **C** is in this case stable enough to allow its observation by EPR (*26*, *27*). This highly reduced state also invokes Mo^{3+}, but has a different charge distribution to state **A**, and the homocitrate remains unprotonated (cf. Table 3). This may explain the observation of a radical attributable to homocitrate for the α-Gln^{195} mutant.

Stereochemistry of Acetylene Protonation. It has long been known that wild-type nitrogenase in D_2O solution reduces C_2H_2 almost exclusively to *cis*-CHD=CHD (*66*). Furthermore, it was recognized from the outset that the lack of products such as CHD=CD_2 rules out the possibility of an acetylide intermediate, although such species have occasionally been mooted in the subsequent literature. The observation that extracted FeMoco also gives primarily *cis*-CHD=CHD when catalyzing the reduction of C_2D_2 (*34*) suggests that this stereospecificity is inherent to the FeMoco, rather than an effect of the protein environment. Indeed, observations on synthetic clusters (*67*) and mononuclear complexes (*68*) show that *cis*-alkene stereochemistry is a routine characteristic of alkyne reduction at metal centers. Detailed experimental studies of the protonation of model alkyne complexes led to the conclusion that the stereochemistry of the alkene product is generally a consequence of the preferred mechanism of protonation of the system (*68*). Thus, the initial site of protonation can be either the metal or the alkyne. In the former case, subsequent migration of the hydride to the alkyne leads to the *cis*-isomer, whereas direct protonation of the alkyne on its more solvent-accessible face gives the *trans*-isomer (Scheme 2). This paradigm is readily applicable to nitrogenase (*2*, *68*). Although wild-type nitrogenase gives only ~4% *trans*-CHD=CHD, mutant forms of the enzyme can give considerably more (*18*, *20*). It was also found that the *cis/trans* isomer ratio is flux-dependent; for both wild type and mutant proteins, the proportion of *trans* isomer increases as the electron flux through the system decreases (*20*). The mutagenesis and electron flux data are consistent with Scheme 2 in that a more electron-rich FeMoco should be more capable of protonation at Fe. Thus, wild-type Av1 and the α-Gln^{195} mutant, discussed above, have normal or near-normal charge densities on FeMoco and so give 5% or less of the *trans* isomer. The α-Ser^{69} mutant also gives a low proportion of *trans* isomer, but has a significantly higher K_m for C_2H_2 reduction (*20*). This perturbation can be assigned to steric rather than electronic effects, as discussed above. Conversely, mutants in which the wild-type α-Arg^{96} residue, which normally places a cationic guanidinium group close to the FeMoco, is replaced by a less basic amino acid are less able to support a charge buildup on FeMoco and so give a little more *trans*-CHD=CHD; the same holds true for the

[5] EPR studies of *A. vinelandii* mutants in which α-Arg^{96} was mutated to Leu, His, Ala, or Gln indicated that these proteins can all bind C_2H_2 at the E_0 redox level (*64*). The α-Arg^{96} side chain, which is cationic at biological pH values, is normally in close contact with S5 of FeMoco. Although the effect of these mutations could be steric in origin, it is also possible that replacing α-Arg^{96} with a less basic residue might perturb the electronic structure of the FeMoco and so allow detectable binding of C_2H_2 at state E_0. This would also explain why isolated FeMoco in the $S = 3/2$ state shows no detectable interaction with C_2H_2 (*65*), even though in this case steric effects should be negligible.

Table 3: Formal Oxidation States in the FeMoco Core Cluster Plus Homocitrate[a] for the Catalytic Intermediates in Scheme 1

enzyme state	formal oxidation states	notes
E_0	$[Fe^{3+}{}_3Fe^{2+}{}_4Mo^{4+}N^{3-}S^{2-}{}_9]^0 \cdot hca^{4-}$	see refs *7*−*9*, *13*, *14*
E_1	$[Fe^{3+}{}_3Fe^{2+}{}_4Mo^{3+}N^{3-}S^{2-}{}_9]^- \cdot hca^{4-}$	CO, C_2H_2 bind reversibly at multiple Fe sites (see Table 2)
E_2	$[Fe^{3+}{}_2Fe^{2+}{}_5Mo^{3+}N^{3-}S^{2-}{}_8(SH)^-]^- \cdot hca^{4-}$	protonation at S2B, see ref *36*
E_3, **A**	$[Fe^{3+}{}_1Fe^{2+}{}_6Mo^{3+}N^{3-}S^{2-}{}_8(SH)^-]^{2-} \cdot hcaH^{3-}$	binds N_2 at Mo in the absence of C_2H_2
E_3, **B**	$[Fe^{3+}{}_2Fe^{2+}{}_5Mo^{4+}N^{3-}S^{2-}{}_8(SH)^-(CHCH_2)^-]^- \cdot hca^{4-}$	transient initial substrate-reduced state
E_3, **C**	$[Fe^{3+}{}_1Fe^{2+}{}_6Mo^{3+}N^{3-}S^{2-}{}_8(S\{H\}CHCH_2)^0]^- \cdot hca^{4-}$	transient for wild-type enzyme, releases C_2H_4

[a] hca^{4-} = fully deprotonated homocitrate.

Scheme 2: Kinetic Control of Product Stereochemistry for Acetylene Reduction in D_2O[a]

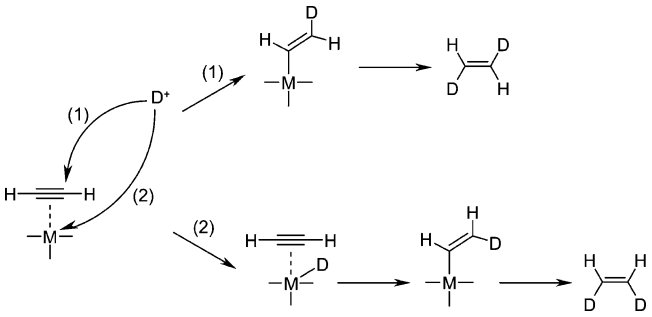

[a] In pathway (1), deuteriation occurs directly on the substrate and leads to the trans-isomer. In pathway (2), initial deuteriation of the metal leads to the cis-product.

α-Asn[195] mutant, except that the effect is more pronounced in this case, for the reasons discussed above. Residue α-Lys[191] is implicated as a component of an electron-transfer pathway from the P-cluster to FeMoco (*47*); hence, a mutation in this residue should impair the electron flux to the FeMoco, resulting in the production of more *trans*-CHD═CHD, as observed (*18*).

An alternative to the mechanisms shown in Scheme 2 is that a proton could be transferred to bound C_2H_2 from one of the central S atoms of the FeMoco rather than from Fe. However, two lines of evidence militate against this. First, the DFT calculations indicate a very high energy barrier for such a transfer. Second, the α-Gln[195] mutant lacks a functional proton channel to S2B, but nevertheless gives very little *trans*-CHD═CHD and also has a K_m for C_2H_2 reduction close to that of the wild-type enzyme.

Production of Ethane from Ethylene and Acetylene. Ethylene is a very poor substrate for nitrogenase (*18*, *21*). This is perhaps surprising given that the enthalpies for addition of H_2 to C_2H_2 and C_2H_4 are both favorable (−42 and −33 kcal mol^{-1}, respectively), whereas the reaction of H_2 with N_2 to give N_2H_2 is endothermic (+51 kcal mol^{-1}), and so N_2 reduction is a much more difficult transformation from a thermodynamic point of view. Evidently, the difficulty with C_2H_4 reduction by nitrogenase arises from a kinetic effect. The DFT calculations discussed above indicate that this is associated with the formation of the initial Fe−CH_2-CH_3 intermediate. Given that the primary route for reduction of C_2H_2 and, by inference, C_2H_4, invokes an iron hydride (Scheme 2), the increased energy cost for production of Fe-CH_2CH_3 compared to Fe−CH═CH_2 should be sufficient to make reduction of C_2H_4 much less competitive against H_2 formation via hydrolysis of the iron hydride intermediate. It should be noted that the reduction cycle for C_2H_2, and by extension C_2H_4, in Scheme 1 involves state E_3, which was assigned to the initial state for binding of N_2 at Mo via homocitrate ring opening (*37*). Hence, the possibility of an alternative route for C_2H_4 reduction on Mo was also considered. Although the formation of a Mo−CH_2CH_3 intermediate should be somewhat more favorable than the corresponding Fe−CH_2CH_3 intermediate, the Mo-bound state cannot relax via migration of the -CH_2CH_3 group to S; hence, the Mo site should be even worse than the Fe sites as a mediator of C_2H_4 reduction.

Under some circumstances, nitrogenase can also catalyze reduction of C_2H_2 to C_2H_6 (*2*, *16*, *18*, *19*). The observation that a α-Lys[191] mutant protein gives no C_2H_6 when turned over under C_2H_4, but does give C_2H_6 when turned over under C_2H_4 plus C_2H_2 (*18*), supports the idea that the reduction of C_2H_2 might provide access to an intermediate not encountered in the reduction of C_2H_4. Specifically, chemical model studies led to the suggestion that protonation of a cofactor-bound -CH═CH_2 intermediate at the α-carbon would lead to C_2H_4, whereas protonation at the *β*-carbon would commit the enzyme to C_2H_6 production (*22*). As noted above, the DFT calculations support this idea, in that protonation at the *β*-carbon of the S−CH═CH_2 intermediate gives an intermediate (**17**) in Figure 3 only 5 kcal mol^{-1} higher in energy than the bound C_2H_4 state resulting from protonation at the α-carbon. Intermediate (**17**) involves a thioaldehyde, stabilized by bridging to the Fe center, and can only be formed from C_2H_2, not from C_2H_4. It is worth noting that the methyl group in (**17**) is free to rotate; hence, the reversible protonation of such a species during the reduction of C_2H_2 in D_2O could result in both an increase in the proportion of *trans*-CHD═CHD and also production of some CHD═CD_2. Very recently, it has been reported that both of these effects occur at pH > 7 (*69*). This is consistent with essentially irreversible protonation at pH 7 but progress toward an equilibrium situation at higher pH.

In conclusion, the model presented here rationalizes the mutagenesis data implicating C_2H_2 reduction on a central face of the FeMoco in terms of migration of the -CH═CH_2 intermediate, initially formed on iron, to sulfur. The model explains both the production of *cis*- versus *trans*-CHD═CHD and C_2H_4 versus C_2H_6 from C_2H_2 in terms of competitive protonation of the FeMoco core cluster and bound hydrocarbon intermediate, at both its α- and *β*-carbons. C_2H_4 is a relatively poor substrate compared to C_2H_2 due to the energetically unfavorable Fe−CH_2CH_3 intermediate required for its reduction. The reduction cycle for C_2H_2 given in Scheme 1 is fully compatible with those for N_2 and H^+ reduction suggested in previous work (*37*, *38*); however, the much easier reduction of C_2H_2 compared to N_2 means that reduction of C_2H_2 can commence before homocitrate ring opening can occur, and hence the Mo atom is not involved in this case.

ACKNOWLEDGMENT

I thank D. J. Lowe, C. J. Pickett, J. R. Sanders, and S. J. George (John Innes Centre), R. A. Henderson (University of Newcastle), and K. Fisher (Virginia Tech) for helpful discussions.

REFERENCES

1. Eady, R. R. (1996) Structure−function relationships of alternative nitrogenases. *Chem. Rev. 96*, 3013−3030.
2. Burgess, B. K., and Lowe, D. J. (1996) Mechanism of molybdenum nitrogenase. *Chem. Rev. 96*, 2983−3011.
3. Howard, J. B., and Rees, D. C. (1996) Structural basis of biological nitrogen fixation. *Chem. Rev. 96*, 2965−2982.
4. Mayer, S. M., Lawson, D. M., Gormal, C. A., Roe, S. M., and Smith, B. E. (1999) New insights into structure−function relationships in nitrogenase: a 1.6 Å resolution X-ray crystallographic study of *Klebsiella pneumoniae* MoFe-protein. *J. Mol. Biol. 292*, 871−891.
5. Peters, J. W., Stowell, M. H. B., Soltis, S. M., Finnegan, M. G., Johnson, M. K., and Rees, D. C. (1997) Redox-dependent structural changes in the nitrogenase P-cluster. *Biochemistry 36*, 1181−1187.
6. Einsle, O., Tezcan, F. A., Andrade, S. L. A., Schmid, B., Yoshida, M., Howard, J. B., and Rees, D. C. (2002) Nitrogenase MoFe-protein at 1.16 Å resolution: a central ligand in the FeMo-cofactor. *Science 297*, 1696−1700.
7. Dance, I. (2003) The consequences of an interstitial N atom in the FeMo cofactor of nitrogenase. *Chem. Commun.* 324−325.
8. Hinnemann, B., and Nørskov, J. K. (2003) Modeling a central ligand in the nitrogenase FeMo cofactor. *J. Am. Chem. Soc. 125*, 1466−1467.
9. Lovell, T., Liu, T. Q., Case, D. A., and Noodleman, L. (2003) Structural, spectroscopic, and redox consequences of central ligand in the FeMoco of nitrogenase: a density functional theoretical study. *J. Am. Chem. Soc. 125*, 8377−8383.
10. Vrajmasu, V., Münck, E., and Bominaar, E. L. (2003) Density functional study of the electric hyperfine interactions and the redox-structural correlations in the cofactor of nitrogenase. Analysis of general trends in ^{57}Fe isomer shifts. *Inorg. Chem. 42*, 5974−5988.
11. Lovell, T., Li, J., Liu, T. Q., Case, D. A., and Noodleman, L. (2001) FeMo cofactor of nitrogenase: a density functional study of states M^N, M^{OX}, M^R, and M^I. *J. Am. Chem. Soc. 123*, 12392−12410.
12. Lee, H.-I., Hales, B. J., and Hoffman, B. M. (1997) Metal-ion valencies of the FeMo cofactor in CO-inhibited and resting state nitrogenase by ^{57}Fe Q-band ENDOR. *J. Am. Chem. Soc. 119*, 11395−11400.
13. Yoo, S. J., Angove, H. C., Papaefthymiou, V., Burgess, B. K., and Münck, E. (2000) Mössbauer study of the MoFe protein of nitrogenase from *Azotobacter vinelandii* using selective ^{57}Fe enrichment of the M-centers. *J. Am. Chem. Soc. 122*, 4926−4936.
14. Pickett, C. J., Vincent, K. A., Ibrahim, S. K., Gormal, C. A., Smith, B. E., and Best, S. P. (2003) Electron-transfer chemistry of the iron−molybdenum cofactor of nitrogenase: delocalized and localized reduced states of FeMoco which allow binding of carbon monoxide to iron and molybdenum. *Chem.-Eur. J. 9*, 76−87.
15. Dilworth, M. J., Eldridge, M. E., and Eady, R. R. (1993) The molybdenum and vanadium nitrogenases of *Azotobacter chroococcum*- effect of elevated temperature on N_2 reduction. *Biochem. J. 289*, 395−400.
16. Kim, C.-H., Newton, W. E., and Dean, D. R. (1995) Role of the MoFe protein alpha-subunit histidine-195 residue in FeMo-cofactor binding and nitrogenase catalysis. *Biochemistry 34*, 2798−2808.
17. Fisher, K., Dilworth, M. J., Kim, C.-H., and Newton, W. E. (2000) *Azotobacter vinelandii* nitrogenases with substitutions in the FeMo-cofactor environment of the MoFe protein: effects of acetylene or ethylene on interactions with H^+, HCN, and CN^-. *Biochemistry 39*, 10855−10865.
18. Fisher, K., Dilworth, M. J., Kim, C.-H., and Newton, W. E. (2000) *Azotobacter vinelandii* nitrogenases containing altered MoFe proteins with substitutions in the FeMo-cofactor environment: effects on the catalyzed reduction of acetylene and ethylene. *Biochemistry 39*, 2970−2979.
19. Scott, D. J., Dean, D. R., and Newton, W. E. (1992) Nitrogenase-catalyzed ethane production and CO-sensitive hydrogen evolution from MoFe proteins having amino acid substitutions in an alpha-subunit FeMo cofactor-binding domain. *J. Biol. Chem. 267*, 20002−20010.
20. Benton, P. M. C., Christiansen, J., Dean, D. R., and Seefeldt, L. C. (2001) Stereospecificity of acetylene reduction catalyzed by nitrogenase. *J. Am. Chem. Soc. 123*, 1822−1827.
21. Ashby, G. A., Dilworth, M. J., and Thorneley, R. N. F. (1987) *Klebsiella pneumoniae* nitrogenase- inhibition of hydrogen evolution by ethylene and the reduction of ethylene to ethane. *Biochem. J. 247*, 547−554.
22. Lowe, D. J., Fisher, K., and Thorneley, R. N. F. (1990) *Klebsiella pneumoniae* nitrogenase- mechanism of acetylene reduction and its inhibition by carbon monoxide. *Biochem. J. 272*, 621−625.
23. Christiansen, J., Seefeldt, L. C., and Dean, D. R. (2000) Competitive substrate and inhibitor interactions at the physiologically relevant active site of nitrogenase. *J. Biol. Chem. 275*, 36104−36107.
24. Christiansen, J., Cash, V. L., Seefeldt, L. C., and Dean, D. R. (2000) Isolation and characterization of an acetylene-resistant nitrogenase. *J. Biol. Chem. 275*, 11459−11464.
25. Shen, J., Dean, D. R., and Newton, W. E. (1997) Evidence for multiple substrate-reduction sites and distinct inhibitor-binding sites from an altered *Azotobacter vinelandii* nitrogenase MoFe protein. *Biochemistry 36*, 4884−4894.
26. Sørlie, M., Christiansen, J., Dean, D. R., and Hales, B. J. (1999) Detection of a new radical and FeMo-cofactor EPR signal during acetylene reduction by the alpha-H195Q mutant of nitrogenase. *J. Am. Chem. Soc. 121*, 9457−9458.
27. Sørlie, M., Christiansen, J., Lemon, B. J., Peters, J. W., Dean, D. R., and Hales, B. J. (2001) Mechanistic features and structure of the nitrogenase alpha-Gln^{195} MoFe protein. *Biochemistry 40*, 1540−1549.
28. Pollock, R. C., Lee, H.-I., Cameron, L. M., Derose, V. J., Hales, B. J., Orme-Johnson, W. H., and Hoffman, B. M. (1995) Investigation of CO bound to inhibited forms of nitrogenase MoFe Protein by ^{13}C ENDOR. *J. Am. Chem. Soc. 117*, 8686−8687.
29. Cameron, L. M., and Hales, B. J. (1998) Investigation of CO binding and release from Mo-nitrogenase during catalytic turnover. *Biochemistry 37*, 9449−9456.
30. George, S. J., Ashby, G. A., Wharton, C. W., and Thorneley, R. N. F. (1997) Time-resolved binding of carbon monoxide to nitrogenase monitored by stopped-flow infrared spectroscopy. *J. Am. Chem. Soc. 119*, 6450−6451.
31. Mayer, S. M., Niehaus, W. G., and Dean, D. R. (2002) Reduction of short chain alkynes by a nitrogenase alpha-70^{Ala}-substituted MoFe protein. *J. Chem. Soc., Dalton Trans.* 802−807.
32. Benton, P. M. C., Laryukhin, M., Mayer, S. M., Hoffman, B. M., Dean, D. R., and Seefeldt, L. C. (2003) Localization of a substrate binding site on the FeMo-cofactor in nitrogenase: trapping propargyl alcohol with an alpha-70-substituted MoFe protein. *Biochemistry 42*, 9102−9109.
33. Bazhenova, T. A., Bazhenova, M. A., Petrova, G. N., Mironova, S. A., and Strelets, V. V. (2000) Catalytic behavior of the nitrogenase iron−molybdenum cofactor extracted from the enzyme in the reduction of C_2H_2 under nonenzymatic conditions. *Kinet. Catal. 41*, 499−510.
34. Bazhenova, T. A., Bazhenova, M. A., Petrova, G. N., and Mironova, S. A. (2002) Kinetics and mechanism of acetylene reduction with europium amalgam catalyzed by isolated active center of nitrogenase. *Kinet. Catal. 43*, 351−362.
35. Ibrahim, S. K., Vincent, K., Gormal, C. A., Smith, B. E., Best, S. P., and Pickett, C. J. (1999) The isolated iron−molybdenum cofactor of nitrogenase binds carbon monoxide upon electrochemically accessing reduced states. *Chem. Commun.* 1019−1020.
36. Durrant, M. C. (2001) Controlled protonation of iron−molybdenum cofactor by nitrogenase: a structural and theoretical analysis. *Biochem. J. 355*, 569−576.
37. Durrant, M. C. (2002) An atomic level mechanism for molybdenum nitrogenase. Part 1. Reduction of dinitrogen. *Biochemistry 41*, 13934−13945.
38. Durrant, M. C. (2002) An atomic level mechanism for molybdenum nitrogenase. Part 2. Proton reduction, inhibition of dinitrogen reduction by dihydrogen, and the HD formation reaction. *Biochemistry 41*, 13946−13955.
39. Chem-X, version 1999.2 (1999) Oxford Molecular Ltd., Oxford, UK.

40. Insight II, version 2000.1 (2000) Accelrys Ltd., Cambridge CB4 0WN, UK.
41. Frisch, M. J., Trucks, G. W., Schlegel, H. B., Scuseria, G. E., Robb, M. A., Cheeseman, J. R., Zakrzewski, V. G., Montgomery, J. A., Jr., Stratmann, R. E., Burant, J. C., Dapprich, S., Millam, J. M., Daniels, A. D., Kudin, K. N., Strain, M. C., Farkas, O., Tomasi, J., Barone, V., Cossi, M., Cammi, R., Mennucci, B., Pomelli, C., Adamo, C., Clifford, S., Ochterski, J., Petersson, G. A., Ayala, P. Y., Cui, Q., Morokuma, K., Malick, D. K., Rabuck, A. D., Raghavachari, K., Foresman, J. B., Cioslowski, J., Ortiz, J. V., Baboul, A. G., Stefanov, B. B., Liu, G., Liashenko, A., Piskorz, P., Komaromi, I., Gomperts, R., Martin, R. L., Fox, D. J., Keith, T., Al-Laham, M. A., Peng, C. Y., Nanayakkara, A., Gonzalez, C., Challacombe, M., Gill, P. M. W., Johnson, B., Chen, W., Wong, M. W., Andres, J. L., Gonzalez, C., Head-Gordon, M., Replogle, E. S., and Pople, J. A. (1998) Gaussian, Inc., Pittsburgh, PA.
42. Berman, H. M., Westbrook, J., Feng, Z., Gilliland, G., Bhat, T. N., Weissig, H., Shindyalov, I. N., and Bourne, P. E. (2000) The protein data bank. *Nucleic Acids Res. 28*, 235−242.
43. Farrugia, L. J. (1997) ORTEP-3 for Windows - a version of ORTEP-III with a graphical user interface (GUI). *J. Appl. Crystallogr. 30*, 565.
44. Pham, D. N., and Burgess, B. K. (1993) Nitrogenase reactivity: effects of pH on substrate reduction and CO inhibition. *Biochemistry 32*, 13725−13731.
45. Lee, H.-I., Cameron, L. M., Hales, B. J., and Hoffman, B. M. (1997) CO binding to the FeMo cofactor of CO-inhibited nitrogenase: ^{13}CO and ^{1}H Q-band ENDOR investigation. *J. Am. Chem. Soc. 119*, 10121−10126.
46. Davies, S. C., Durrant, M. C., Hughes, D. L., Richards, R. L., and Sanders, J. R. (2000) Iron, cobalt and vanadium complexes of the $N(CH2CH2S)_3^{3-}$ ligand with chloride, azide, cyanide and carbonyl co-ligands. *J. Chem. Soc., Dalton Trans.* 4694−4701.
47. Grönberg, K. L. C., Gormal, C. A., Durrant, M. C., Smith, B. E., and Henderson, R. A. (1998) Why R−Homocitrate is essential to the reactivity of FeMo-cofactor of nitrogenase: studies on $NifV^-$-extracted FeMo-cofactor. *J. Am. Chem. Soc. 120*, 10613−10621.
48. Christie, P. D., Lee, H.-I., Cameron, L. M., Hales, B. J., Orme-Johnson, W. H., and Hoffman, B. M. (1996) Identification of the CO-binding cluster in nitrogenase MoFe protein by ENDOR of ^{57}Fe isotopomers. *J. Am. Chem. Soc. 118*, 8707−8709.
49. Thorneley, R. N. F., and George, S. J. (2000) in *Prokaryotic Nitrogen Fixation: A Model System for Analysis of a Biological Process* (Triplett, E. W., Ed.) pp 81−91, Horizon Scientific Press, Wymondham, UK.
50. Maskos, Z., and Hales, B. J. (2003) Photolability of CO bound to Mo-nitrogenase from *Azotobacter vinelandii*. *J. Inorg. Biochem. 93*, 11−17.
51. Cui, Z., Dunford, A. J., Durrant, M. C., Henderson, R. A., and Smith, B. E. (2003) Binding sites of nitrogenase: kinetic and theoretical studies of cyanide binding to extracted FeMo-cofactor derivatives. *Inorg. Chem. 42*, 6252−6264.
52. Makitra, R. G., Protsailo, T. A., Boldeskul, I. E., and Rozhkova, Z. Z. (1982) Influence of nature of solvent on IR and NMR spectra of ethyl cyanoacetate and formaldehyde. *J. Appl. Spectrosc. (English Translation) 37*, 1272−1277.
53. Hitchcock, P. B., Lappert, M. F., and McGeary, M. J. (1990) Dimetallostannylene transition metal complexes. *Organometallics 9*, 884−886.
54. Rakowski Dubois, M. (1989) Catalytic applications of transition metal complexes with sulfide ligands. *Chem. Rev. 89*, 1−9.
55. Maeyama, M., Sakane, G., Pierattelli, R., Bertini, I., and Shibahara, T. (2001) Adduct of acetylene at sulfur in an oxygen- and sulfur-bridged open cubane cluster complex of tungsten. *Inorg. Chem. 40*, 2111−2119.
56. Maeyama, M., and Shibahara, T. (2001) Reaction of a sulfur bridged incomplete cubane-type tungsten cluster with acetylene: formation of three carbon−sulfur bonds. *Chem. Lett.*, 120−121.
57. Bentrop, D., Bertini, I., Borsari, M., Cosenza, G., Luchinat, C., and Niikura, Y. (2000) A refined model for $[Fe_3S_4]^0$ clusters in proteins, *Angew. Chem., Int. Ed. 39*, 3620−3622.
58. Davis, L. C., Henzl, M. T., Burris, R. H., and Orme-Johnson, W. H. (1979) Iron−sulfur clusters in the molybdenum−iron protein component of nitrogenase. Electron paramagnetic resonance of the carbon monoxide inhibited state. *Biochemistry 18*, 4860−4869.
59. Lowe, D. J., Eady, R. R., and Thorneley, R. N. F. (1978) Electron paramagnetic resonance studies on nitrogenase of *Klebsiella pneumoniae*. Evidence for acetylene- and ethylene-nitrogenase transient complexes. *Biochem. J. 173*, 277−290.
60. Newton, W. E., Fisher, K., Kim, C.-H., Shen, J., Cantwell, J. S., Thrasher, K. S., and Dean, D. R. (1995) in *Nitrogen Fixation: Fundamentals and Applications* (Tikhonovich, I. A., Provorov, N. A., Romanov, V. I., Newton, W. E., Ed.) pp 91−96, Kluwer, Dordrecht.
61. McLean, P. A., Smith, B. E., and Dixon, R. A. (1983) Nitrogenase of *Klebsiella pneumoniae* NifV mutants- investigation of the novel carbon monoxide-sensitivity of hydrogen evolution by the mutant enzyme. *Biochem. J. 211*, 589−597.
62. McLean, P. A., and Dixon, R. A. (1981) Requirement of *NifV* gene for production of wild-type nitrogenase enzyme in *Klebsiella pneumoniae*. *Nature 292*, 655−656.
63. McLean, P. A., True, A., Nelson, M. J., Lee, H.-I., Hoffman, B. M. and Orme-Johnson, W. H. (2003) Effects of substrates (methyl isocyanide, C_2H_2) and inhibitor (CO) on resting-state wild-type and $NifV^-$ *Klebsiella pneumoniae* MoFe proteins. *J. Inorg. Biochem. 93*, 18−32.
64. Benton, P. M. C., Mayer, S. M., Shao, J. L., Hoffman, B. M., Dean, D. R., and Seefeldt, L. C. (2001) Interaction of acetylene and cyanide with the resting state of nitrogenase alpha-96-substituted MoFe proteins. *Biochemistry 40*, 13816−13825.
65. Grönberg, K. L. C., Gormal, C. A., Smith, B. E., and Henderson, R. A. (1997) A new approach to identifying substrate binding sites on isolated FeMo-cofactor of nitrogenase. *Chem. Commun.* 713−714.
66. Dilworth, M. J. (1966) Acetylene reduction by nitrogen-fixing preparations from *Clostridium pasteurianum*. *Biochim. Biophys. Acta 127*, 285−294.
67. Laughlin, L. J., and Coucouvanis, D. (1995) Use of $[MoFe_3S_4]^{3+}$ single cubanes in the catalytic reduction of acetylene to ethylene and ethane. Identification of molybdenum and iron atoms as catalytic sites during substrate reduction and implications for nitrogenase action. *J. Am. Chem. Soc. 117*, 3118−3125.
68. Henderson, R. A. (1996) Protonation of unsaturated hydrocarbon ligands: Regioselectivity, stereoselectivity, and product specificity. *Angew. Chem., Int. Ed. Engl. 35*, 947−967.
69. Han, J., and Newton, W. E. (2004) Differentiation of acetylene-reduction sites by stereoselective proton addition during *Azotobacter vinelandii* nitrogenase-catalyzed C_2D_2 reduction. *Biochemistry 43*, 2947−2956.

BI036300L